where

$$\Psi = \frac{\sum_{n=1}^{N} \sin\psi_n}{\sum_{n=1}^{N} \cos\psi_n}$$

$$a_{in} = \frac{\Phi_{in} f_n}{m_n[(\omega_n{}^2 - \omega^2)^2 + (2\omega_n\omega\zeta_n)^2]^{1/2}}$$

$$\psi_n = \tan^{-1}\frac{2\omega_n\,\omega\zeta_n}{\omega_n{}^2 - \omega^2} \qquad (2)$$

where Φ_{in} and w_i mean the ith entry of the nth modal vector and displacement vector, respectively. Each ζ_n can be determined from the frequency response curves, noting that the maximum acceleration (for light damping) at the jth natural frequency is

$$\{\ddot{w}\}_{\max} = \{\Phi\}_j f_j/2m_j\zeta_j \qquad (3)$$

The quantities m_j, f_j, and $\{\Phi\}_j$ were determined from the finite element computer program, and ζ_j was then calculated from Eq. (3), using $\{\ddot{w}\}_{\max}$. The results, comparing frequency transfer functions, show good agreement with the experiment, using the first 10 modes.

The plate was then driven by a random signal at point (13,9). Accelerations were monitored at locations (24,0) and (24,9). The system used consisted of a Calidyne 150 pound shaker, a General Radio Noise generator, and an MB Electronics T388 Automatic Equalization System. The input was a "flat" band limited signal of level 0.00125 lb²/cps and 500 cps bandwidth presented in Figs. 2 and 3. It was impossible to equalize the input spectrum so that the spectrum at the shaker table was flat, because the equalization filters had a gain of only ±40 db relative to each other. Resonances with gains of 40 db occurred, so the signal occasionally would exceed the limits of the filter amplifiers. This made the input spectrum rough. Thirty seconds of data from the shaker table and each of the two accelerometers were recorded on analog tape and then digitized. The sampling rate was 5 kc and fixed the Nyquist frequency at 2.5 kc.

The random data were analyzed for their spectral density according to the modified periodogram approach proposed by Welch.[3] The data window used in this analysis was the function

$$D(t) = 1 - |t|/T \quad |t| \leq T$$
$$= 0 \quad |t| > T \qquad (4)$$

which is the Parzen spectral window. The equivalent window bandwidth (EBW) is $\Delta\omega = 16.1/\tau(L + 1)$, where the total record is broken up into L segments which overlap each other halfway. The modified periodogram was calculated for each segment sequentially and the L modified periodograms were averaged. The variance of the PSD can be given by equivalent degrees of freedom (EDF) which is EDF = 3.6 N/(L−1)

For the tests conducted, $\Delta f = \Delta\omega/2\pi = 3.1$ cps and EDF = 130. The bandwidth is narrow enough to resolve most of the peaks, and the variance is low.

Results and comparisons to theory

It is shown in Thompson[7] and elsewhere that

$$S_a(\omega) = |H(\omega)|^2\, S_f(\omega) \qquad (5)$$

Figures 2 and 3 present this relationship. Analytically derived $S_a(\omega)$ from Eq. (1) were used to construct the triangular points on these figures, using Eq. (5) and the input shown in Figs. 2 and 3 as thin lines. The heavy solid lines represent completely experimental $S_a(\omega)$ data. The agreement appears adequate.

There are points which do not agree well with the experiment at the resonant peaks. There is an overshoot of the analytically derived spectra at these frequencies, which is quite severe. This is mainly caused by "leakage." From the experimental input curve, it can be seen that neighboring each peak is a deep valley. As the Parzen window is convolved onto the true experimental spectrum, the presence of the valleys is felt at adjacent peaks, and vice versa. Even a 3.1 cps bandwidth window cannot compensate for the total test dynamics. The spectrum calculated by Eq. (5), has, in effect, skipped the final windowing that was unavoidably done to the experimental spectrum. When the force spectrum in Fig. 2 or 3 is physically passed through the plate, it has the plate dynamics superimposed on it. These dynamics tend to "roughen" the experimental spectrum, which is then unavoidably windowed in the process of deriving Figs. 2 and 3.

Further proof of this hypothesis is provided by Fig. 3 which is the acceleration PSD at (24,9). The transfer function for this plot is smoother than the others, and consequently the data agree better. The analytical curve in Fig. 3 still is somewhat inaccurate at certain resonances, however. These are instances where the analytic transfer functions are inaccurate.

It is felt that the only effective cure for this problem is to prewhiten the data by applying a series of prewhitening filters to flatten the spectrum. However, raw data must be analyzed, then prewhitened on the basis of the raw data analysis, then the PSD computed again. The final PSD can be postdarkened to resemble the true spectrum.

References

[1] Anderson, R. G. et al., "Vibration and Stability of Plates Using the Finite Element Method," *International Journal of Solids and Structures*, Vol. 4, No. 10, pp. 1031–1055.

[2] Claassen, R. W. and Thorn, C. J., "Vibrations of a Rectangular Cantilever Plate," PMR TR 61-1, Aug. 1962, Pacific Missile Range, Point Mugu, Calif.

[3] Welch, P. W. et al., "The Fast Fourier Transform and Its Applications," Research Paper R. C. 1743, 1967, IBM, Yorktown Heights, N. Y.

[4] Eringen, A. C., "Response of Beams and Plates to Random Loads," *Transactions of ASME*, Series E, Vol. 24, No. 1, 1957, pp. 46–52.

[5] Newsom, C. D., Fuller, J. R., and Sherrer, R. E., "A Finite Element Approach for the Analysis of Randomly Excited, Complex, Elastic Structures," *Joint AIAA-ASME Conference on Structures, Structural Dynamics and Materials*, 1967, pp. 125–32.

[6] Stanisic, M. M., "Response of Plates to Random Load," *Journal of Acoustical Society of America*, Vol. 43, No. 6, 1968, pp. 1351–7.

[7] Thompson, W. T., "Continuous Structures Excited by Correlated Random Forces," *International Journal of Mechanical Sciences*, Vol. 4, March–April 1962, pp. 109–14.

[8] Trubert, M. R. P., "Response of Structures to Statistically Correlated Multiple Random Excitations," *Journal of the Acoustical Society of America*, Vol. 35, No. 7, 1963, pp. 1009–22.

[9] Zienkiewicz, O. C. and Cheung, Y. K., *The Finite Element Method*, McGraw-Hill, London, 1967, p. 92.

Fog Dispersal By High-Power Lasers

GEORGE W. SUTTON*

Avco Everett Research Laboratory, Everett, Mass.

Nomenclature

a = sound speed $(\gamma kT/M)^{1/2}$
A = constant, Eq. (22)
c_p = specific heat at constant pressure

Received June 9, 1970; revision received July 22, 1970. This work was supported by the AVCO Independent Research and Development Program.

* Scientist. Fellow AIAA.

C = mass concentration
$\mathfrak{D}$ = diffusion coefficient for water vapor
f = droplet size distribution function
h_v = heat of vaporization
H = total enthalpy
I = radiant intensity
k = Boltzmann constant
Le = Lewis number
m = mass vaporization rate per unit area
M = mass of water molecule
$\mathfrak{N}$ = number density of water vapor
n = index of refraction
N = number density
p = pressure
Q = cross section
r = droplet radius
t = time
T = temperature
u = propagation speed
x = propagation direction
Z = $\rho_f(x,t)/\rho_l$
α = droplet absorption coefficient
β = see Eq. (14)
γ = ratio of specific heats
ϵ = permittivity
ρ = mass density
ϕ = correction factor for heat conduction to air
λ = wavelength
η = thermal conductivity

Subscripts

a = absorption
f = fog
g = air
l = liquid
0 = surface
s = scattering
v = vapor
∞ = initial values

Superscripts

$'$ = real
$''$ = imaginary

Introduction

IN this Note, the dispersal of fog by high-power pulsed lasers is considered. Fog dispersal measurements with a N_2-CO_2 laser at low cw powers (~50 w/cm²) have been reported; however, natural convection started after about 1 sec so that continuous removal of the convected fog was required.[1] On the other hand, very high-power pulses do not necessarily heat the air by conduction, and may disperse the fog along the path of propagation.

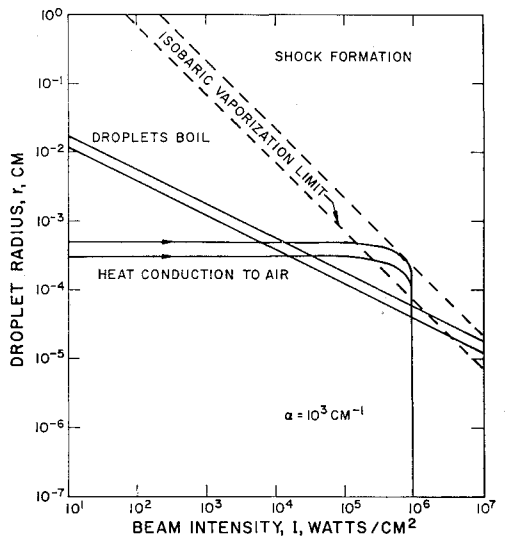

Fig. 1 Vaporization regimes of water droplets.

Vaporization Regimes

To clarify the vaporization regimes of interaction of droplets with lasers at high powers, see Fig. 1. Heat conduction is negligible for[2]

$$r^2 I \alpha c_p / 3\eta h_v > 1 \tag{1}$$

However, above this line, the equilibrium temperature of a droplet can approach the boiling point. This can be seen from the diffusion equation, whose solution for a sphere is[2]

$$e^{rm/\rho_g \mathfrak{D}} = (1 - C_\infty)/(1 - C_0) \tag{2}$$

hence $C_0 \approx 1$ when

$$rm/\rho_g \mathfrak{D} \approx 1 \tag{2a}$$

We next evaluate the vaporization rate. Neglecting heat conduction, the steady-state energy equation for a sphere is

$$4\pi r^2 m h_v = I Q_a \tag{3}$$

where the cross sections for absorption are given by

$$Q = (\tfrac{4}{3})\pi r^3 \alpha \tag{4}$$

and where α is the attenuation coefficient in the liquid. Combining Eqs. (3) and (4)

$$m = rI\alpha/3h_v \tag{5}$$

Thus, from Eqs. (2a) and (5) we can expect the water droplet temperature to be close to the boiling point when

$$r^2 I \alpha / 3\rho_g h_v \mathfrak{D} \geq 1 \tag{6}$$

This line is also shown in Fig. 1. Equations (1) and (6) differ only by the Lewis number. Thus, in the region where heat conduction is negligible, the droplet is close to the boiling point.

Equation (2) does not apply for very high vaporization rates, since the evaporation rate becomes limited to the ratio of the local vapor pressure to the sound speed in the vapor; specifically,[2]

$$m = (\gamma/2\pi)^{1/2} p_v / a_v \tag{7}$$

Combining Eqs. (5) and (7)

$$p_v = (2\pi/\gamma)^{1/2} a_v r I \alpha / 3h_v \tag{8}$$

The boundary for vaporization limitation occurs when $p_v = p_\infty$, e.g.,

$$rI\alpha = 3(\gamma/2\pi)^{1/2} p_\infty h_v / a_v \tag{9}$$

which is also shown in Fig. 1. Above this line the diffusion solution, Eq. (2), does not apply. For even higher heating rates than given by Eq. (9), the vapor pressure near the sur-

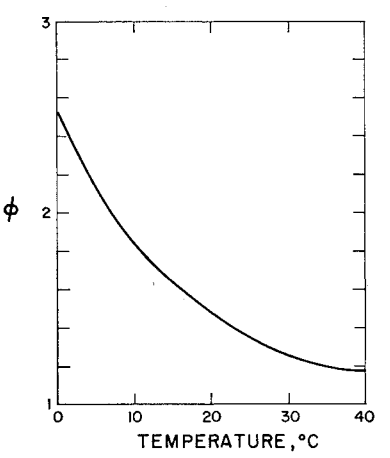

Fig. 2 Heat conduction correction for saturated air.

Table 1 Real and imaginary index of refraction of water at 10.6 μm

	n'	n''	α, M^{-1}
Hermann[3]; Mullaney et al.[1]	1.193	0.102[a]	0.12×10^6
Pontier and Dechambenoy[5]	1.166	0.0850	$0.94^a \times 10^6$
Zuev, Lopasov, and Sonchik[6]	1.15	0.08	$0.94^a \times 10^6$

[a] Calculation from Eq. (12).

face will rise above the background pressure, and can cause shock waves to propagate out from the droplet. We can define this boundary from considering the momentum of the vapor, e.g.,

$$\Delta p = p_v - p_\infty = \rho_v u^2 \equiv m^2/\rho_v \tag{10}$$

We may set $\Delta p = p_\infty$ as a criterion for such shock formation; then with the use of Eq. (7) and the perfect gas law, Eq. (10) yields

$$rI\alpha = 3(2\gamma)^{1/2} h_v p_\infty / a_v \tag{11}$$

Equation (11) is also shown on Fig. 1. Above this line we may expect shock waves to propagate out from the droplet. Notice that the criteria for shock waves is only a factor of $(4\pi)^{1/2}$ greater than the criteria for boiling given by Eq. (9).

Dispersal Propagation

We next determine the propagation profile of a high-power N_2-CO_2 laser into the fog, that is, the variation of beam intensity and fog density in the direction of propagation. When the laser is first turned on, the fog near the laser vaporizes first. The laser beam can then reach fog further away and vaporize it. Thus, after an initial transient, a fog dispersal front propagates away from the laser with a propagation speed u. This speed is obviously given by the inverse ratio of the enthalpy per unit volume needed to clear the fog, to the beam intensity. To obtain the fog profile in the direction of propagation, we make several simplifying assumptions: a) in the absence of fog, the laser beam is of uniform intensity; b) the beam power is sufficiently large and the pulse time sufficiently short that winds and natural convection are negligible; and c) the scattering cross section of the fog is small compared to the absorption cross section. This last assumption is based on the peak fog particle radius of about 3 μm and a median radius of 5 μm. For the wavelength of the N_2-CO_2 laser, 10.6 μm, the index of refraction[3] of liquid water is 1.193. The scattering and absorption cross sections are given by[4] (for $r \ll \lambda$)

$$Q_a = (24\pi^2 r^3/\lambda)\epsilon''[(\epsilon' + 2)^2 + \epsilon'^2] = \tfrac{4}{3}\pi r^3 \alpha \tag{12}$$

$$Q_s = \tfrac{8}{3}(16\pi^2/9)|\beta|^2 \pi r^2 (2\pi r/\lambda)^4 \tag{13}$$

where

$$\beta = 3(\epsilon - 1)/4\pi(\epsilon + 2) \tag{14}$$

and

$$\epsilon = n^2 \tag{15}$$

Some values of n', n'' and α from various references are shown in Table 1. Reference 6 contains a summary of other measurements of n' and n''. Equations (12) and (13) are applicable only if the skin depth is much greater than the droplet radius, e.g., $4\pi n'' r/\lambda \ll 1$. Thus, Eq. (12) applies only if $r \ll 10$ μm. Using the values in Table 1 and Eqs. (12) and (13) the absorption exceeds the scattering when $r \lesssim 3$ μm. This is in close agreement with more exact calculations[3] for $\alpha = 10^{-1}$ and $n' = 1.187$, which predicts that $Q_a/Q_s > 1$ for $r < 5$ μm. Although fog particles greater than 5 μm scatter more than they absorb, their relative number density is small. In addition, the time rate of decrease of radius is linearly proportional to the particle radius so that

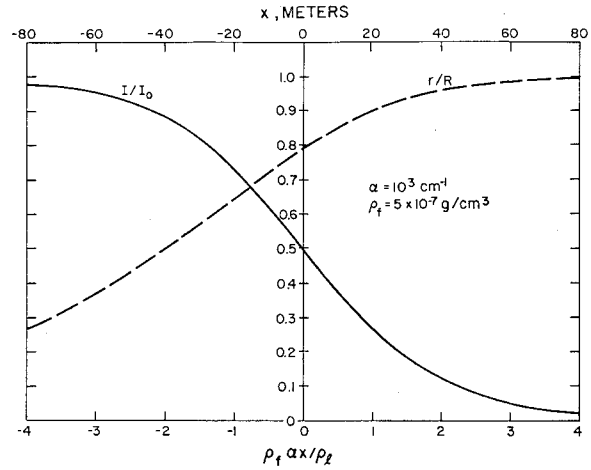

Fig. 3 Intensity profile in fog.

large particles vaporize more rapidly than do small particles. Thus, the assumption that scattering may be neglected for fogs is physically justified.

To obtain the profiles, the energy and radiation equations are solved. For convenience, the former is written in spatial coordinates moving with the fog dispersal front at velocity u. These equations are, respectively,

$$-\rho_g u(dH/dx) = I\langle NQ_a\rangle \tag{16}$$

$$dI/dx = -I\langle NQ_a\rangle \tag{17}$$

The negative sign in Eq. (16) occurs because x is chosen in the direction of propagation. In this moving frame, the fog is moving in the negative direction with speed u. To obtain the total absorption cross section $\langle NQ_a\rangle$ we define a distribution function $f(r)$ for the fog particles such that the number density of fog particles with radius between r and $r + dr$ is given by $f(r)dr$. The total number density is, therefore

$$N = \int_0^\infty f(r)dr \tag{18}$$

The fog mass density is then

$$\rho_f = \frac{4}{3}\pi\rho_l \int_0^\infty f(r) r^3 dr \tag{19}$$

The total cross section is obtained from Eq. (12)

$$\langle NQ_a\rangle = \frac{4}{3}\pi\alpha \int_0^\infty f(r) r^3 dr = \frac{\alpha\rho_f}{\rho_l} \equiv \alpha Z \tag{20}$$

using Eq. (18). The total enthalpy per unit mass of air given by

$$H = \int c_p dT + h_v(\rho_{f\infty} - \rho_f)/\rho_g \tag{21}$$

where c_p and ρ are the specific heat and mass density of the saturated air. In the regime defined by Eq. (6) where heat conduction is negligible, we may neglect the first term of Eq. (21). To relate the gas temperature T to the fog density, use is made of the equilibrium vapor pressure relation which becomes

$$[\mathfrak{R}_\infty + (\rho_{f\infty} - \rho_f)/M]kT = A \exp(-h_v M/kT) \tag{22}$$

Taking the derivative of Eq. (22) one obtains, for $h_v M/kT \gg 1$

$$d\rho_f/dx = (\rho_{f\infty} M^2 h_v/k^2 T^3)(dT/dx) \tag{23}$$

Combination of Eqs. (16, 17, 19, 21, and 23) yields

$$\rho_l h_v u\phi(dZ/dx) = I\alpha Z,\ dI/dx = -I\alpha Z \tag{24}$$

where

$$\bar{\phi} = [1 + \rho_g c_p T(kT/Mh_v)^2 p_v^{-1}]_\infty \tag{25}$$

We note that except for the Lewis number, the expression for ϕ is the same as that inferred from Ref. 2 for inclusion of heat conduction from the droplet into the surrounding air, e.g.,

$$\phi = 1 + \rho_g c_p T(kT/Mh_v)^2 p_v^{-1} Le^{-1} \quad (26)$$

If the Lewis number is less than unity, then the heat conduction is sufficient to prevent recondensation of the air in the heat conduction regime. However, the Lewis number for the diffusion of water vapor is about 1.5; hence the heat conduction from the droplet is not quite sufficient to prevent recondensation, contrary to Ref. 1. In the regime where heat conduction can be neglected, the heat absorbed by the droplet vaporization is definitely not sufficient to prevent recondensation.

If the regime of operation in Fig. 1 is such that conduction to the air is negligible, then $\phi = 1$. For the regime where conduction must be considered, ϕ is shown as a function of temperature for saturated air in Fig. 2.

The boundary conditions for Eq. (24) are

$$x = \infty, I = 0, \rho_f = \rho_{f\infty}, x = -\infty, I = I_0, \rho_p = 0 \quad (27)$$

and we arbitrarily set $I = \frac{1}{2}I_0$ at $x = 0$. The solution to Eqs. (24), subject to Eq. (27) is

$$\rho_f(x)/\rho_{f\infty} = 1 - I(x)/I_0 \quad (28)$$

$$I(x)/I_0 = [1 - \exp(\alpha\rho_f x/\rho_l)]^{-1} \quad (29)$$

$$u = I_0/\rho_f h_v \phi \quad (30)$$

Above the boiling line in Fig. 1, h_v must be increased by about 12% (at room temperature) to account for the additional energy to heat the droplet to its boiling point. In addition, it can be shown that for any given droplet

$$r(x)/r_\infty = [\rho_f(x)/\rho_{f\infty}]^{1/3} \quad (31)$$

Equations (29) and (31) are shown in Fig. 3.

The time-dependent solution of the equations in stationary coordinates x' been derived independently by Glickler.[7] His results are

$$I(x',t)I_0 = \{1 + [\exp(Z_0\alpha x') - 1]\exp(-\alpha t I_0/h_v\rho_l)\}^{-1} \quad (32)$$

Equation (32) reduces to the quasi-stationary solution, Eq. (29), in those parts of the fog where $I(x',0) \ll I_0$.

Scattering by Vaporized Droplet

After the droplet is vaporized, and before diffusion sets in, the vapor will occupy a spherical volume of radius $R \sim 10r$. This causes elastic scattering, whose cross section is[8]

$$Q_{sv} = 2\pi k^2(\Delta n)^2 R^4 \quad (33)$$

which decreases with time due to diffusion. For a typical fog droplet the time for diffusion to cause an appreciable change in Q_{sv} is

$$t \approx 10^{-2}[4N^{2/3}\mathfrak{D}]^{-1} \quad (34)$$

For example, if $N = 10^3$, $t \approx 10^{-4}$ sec.

Discussion

The profiles shown in Fig. 3 are somewhat different than those given in the past. For example if ρ_f is constant, Eq. (24) predicts that

$$I/I_0 = \exp(-\alpha\rho_f x/\rho_l) \quad (35)$$

We see that Eq. (29) has this behavior as $x \to \infty$. On the other hand, if the intensity is constant, then the fog density decreases exponentially with distance. Thus the solution, Eqs. (28) and (29), bridges the two limiting solutions of constant intensity and constant fog density.

It is instructive to consider the history of some typical droplets as they vaporize; to do this, we have plotted Eq. (31) on Fig. 1 for two typical initial drop sizes, 3 and 5 μm, for $I_0 = 10^6$ w/cm^2. The undisturbed fog is at the left; initially the droplet is in the heat conduction regime. As the beam propagates into the fog, the radius decreases and the droplet moves into the vaporization limit region, almost reaching the shock line. As the droplet radius decreases further, the droplet moves back into the heat conduction regime.

As an example, consider an extremely dense fog of 0.5×10^{-6} g/cm^3. For a beam intensity of 10^6 w/cm^2, the propagation speed is about 6.7×10^6 M/sec. Consider a pulse time of 10^{-4} sec. The beam will propagate about 0.67 km. From Eq. (33) we may estimate the extinction length for the vaporized droplet, using $(n - 1) = 2.73 \times 10^{-4}$ for air and 1.83×10^{-4} for water vapor[9] at one atmosphere and 100°C, and assuming a Gaussian distribution of fog droplet initial radii. The result is that the extinction length is 7 km. Since this is much larger than the distance propagated, scattering by vaporized droplets is negligible. Since the vapor droplets diffuse after about 100 μsec, longer pulse times and fog dispersion lengths should be possible. An interesting question is the subsequent history of the vaporized fog droplets as they begin to recondense, but this question is beyond the scope of the present Note.

References

[1] Mullaney, G. J., Christiansen, W. H., and Russell, D. A., "Fog Dissipation Using a CO_2 Laser," *Applied Physics Letters*, Aug. 15, 1968, pp. 145–147.

[2] Williams, F. A., "On Vaporization of Mist by Radiation," *International Journal of Heat and Mass Transfer*, Vol. 8, pp. 575–587.

[3] Herman, B. M., "Infrared Absorption, Scattering, and Total Attenuation Cross Sections for Water Spheres," *Quarterly Procedures of the Royal Meteorological Society*, Vol. 88, 1962, p. 143.

[4] Landau, L. D. and Lifshitz, E. M., *Electrodynamics of Continuous Media*, Pergamon Press, New York, 1960.

[5] Pontier, L. and Dechambenoy, C., "Determination des Constantes Optiques de L'eau Liquide Entre 1 et 40 μ," *Annals of Geophysics*, Vol. 22, No. 4, 1966, pp. 633–641.

[6] Zuev, V. E., Lopasov, V. P., and Sonchik, V. K., "Experimental Study of the Complex Index of Refraction of Water in the Spectral Range of 2.5 to 25 μ," *Izvestiya Akademii Nauk SSSR (Seriya) Fizika Atmosfery I Okeana (Bulletin of the Academy of Sciences of the USSR, Atmospheric and Oceanic Physics)*, Vol. 3, No. 1, Jan. 1967, pp. 16–24.

[7] Glickler, S. L., "Propagation of a 10.6 micron Laser through a Cloud including Droplet Vaporization," to be published in *Journal of Applied Optics*.

[8] Van de Hulst, H. C., *Light Scattering by Small Particles*, Wiley, New York, 1957.

[9] Greenfield, M. A., "Calculation of Index of Refraction of Gases from Absorption Data, *Journal of the Optical Society of America*, Vol. 40, No. 10, October 1950.

Unsteady Radiation Slip

VEDAT S. ARPACI*
University of Michigan, Ann Arbor, Mich.

Introduction

ALTHOUGH increased attention has been paid in the last decade to problems of radiating gas, the related boundary conditions so far appear to have received inadequate treatment. This is probably caused by the fact that the astrophysicist and the gas dynamicist are not primarily concerned with boundaries, and the boundary layer specialist has been often forced, because of the complexity of his problems, to consider only black surfaces. It is the purpose of this study to discuss conditions for diffuse nongray boundaries of un-

Received March 5, 1970; revision received June 18, 1970.

* Professor, Department of Mechanical Engineering.